J. Appl. Comput. Mech., xx(x) (2026) 1-10
DOI: 10.22055/jacm.2026.48692.5432

ISSN: 2383-4536
jacm.scu.ac.ir

Shahid Chamran University of Ahvaz

Journal of Applied and Computational Mechanics

Research Paper

Influence of Strut Cross-section on Haemodynamics and Drug Transport in Stent-based Therapy

Kimiya Kasaeinia[1], Rafat Mohammadi[1], Ali Seyedhosseini[1], Pujith R.S. Vijayaratnam[2], Tracie J. Barber[2]

[1] Department of Mechanical Engineering, Arak University, Arak, Iran,
Email: Kimiya.kasaei@gmail.com (K.K.); r-mohammadi@araku.ac.ir (R.M.); Aliseyyedhosseini75@gmail.com (A.S.)

[2] School of Mechanical and Manufacturing Engineering, University of New South Wales, Sydney, Australia,
Email: p.vijayaratnam@unsw.edu.au (P.R.S.V.); t.barber@unsw.edu.au (T.J.B.)

Received August 16 2025; Revised November 07 2025; Accepted for publication January 04 2026.
✉ Corresponding author: R. Mohammadi (r-mohammadi@araku.ac.ir)

Abstract. Drug-eluting stents effectively treat stenotic vascular diseases, yet their struts can disturb blood flow and promote restenosis. Stent geometry, therefore, plays a crucial role in balancing haemodynamics with drug delivery. This study compared streamlined and non-streamlined strut cross-sections within an ideal coronary artery model using computational fluid dynamics. Strut height, width, and aspect ratio were analyzed for their effects on flow and drug transport. Results showed taller struts worsened restenosis risk but increased flow-mediated drug uptake, while greater width enhanced contact-mediated uptake. Streamlined profiles improved haemodynamics but reduced flow-mediated delivery. Among designs with equal perimeter, circular arc struts with an aspect ratio of two achieved the highest overall drug uptake; however, this configuration also increased regions of low wall shear stress, highlighting the clinical trade-off between maximising drug delivery and maintaining favourable haemodynamics.

Keywords: Drug-eluting stents, Haemodynamics, Drug delivery, Stent design, Computational fluid dynamics.

1. Introduction

Coronary artery disease is the leading cause of death worldwide. Although percutaneous transluminal angioplasty with stent placement is the standard method for restoring blood flow in blocked arteries, its effectiveness is often reduced by the frequent occurrence of restenosis. To combat this problem, drug-eluting stents (DESs) have been created. These stents gradually release antiproliferative drugs, such as sirolimus, paclitaxel, and everolimus, to prevent excessive cell growth and tissue buildup [1].

Notable studies have focused on luminal factors influencing drug distribution as well as the relationship between DES thrombosis and stent design [2, 3], dimensions, apposition [4], overlap [5], drug combinations [6, 7], and interactions. Simulation results of steady-state drug uptake under idealized luminal blood flow conditions [5, 8] revealed that the drug released from non-contacting strut surfaces also contributes to total drug deposition, which explains the increased tissue deposition. Elevated uptake was expected as strut-induced flow recirculation zones act as minimally diluted drug pools. As secondary sources of tissue uptake, these pools produce significant drug concentrations at the lumen–tissue interface [8]. However, our previous study showed that the upstream recirculation zone enhanced drug uptake, but the downstream recirculation zone extracted drug from the tissue [9]. Therefore, strut dimensions and stent design, in addition to affecting the primary neointimal hyperplastic response, also change the amount of drug uptake by affecting the size of the pools [8, 10].

The majority of early stent designs focused on wire coil struts, characterized by a circular cross-sectional strut, and slotted tube stents, featuring a rectangular cross-sectional strut [11]. These struts always induce flow disturbances in their surrounding environment. Additionally, multiple researchers [12, 13] examined the haemodynamic impact of bare-metal stents with varying cross-sectional shapes, strut heights, and strut widths on haemodynamics and suggested that reducing the strut height and modifying the stent strut profile to a more streamlined shape can improve haemodynamics for successful clinical stenting using two-dimensional flow simulations. While extensive research has explored the impact of stent strut geometry on drug release and deposition, the specific influence of strut aspect ratio (AR, the ratio of width to height) in various cross-sectional strut profiles on haemodynamics and drug transport in DESs remains understudied. While prior research has examined the effects of strut height [12], width [14], or profile shape [13] individually, the combined influence of strut AR across both streamlined and non-streamlined geometries has received limited attention. Moreover, few studies have systematically compared how these geometric factors interact to affect both recirculation dynamics and drug uptake within a unified computational framework.

Published online: January 07 2026

Table 1. Parameters of strut geometry (variation of height and width).

Geometry case	Cross-sectional shape	Strut height h (mm)	Strut width w (mm)
Case A	RT	0.05	0.1
Case B	RT	0.025	0.1
Case C	RT	0.0125	0.1
Case D	RT	0.05	0.14
Case E	CA	0.05	0.1
Case F	CA	0.025	0.1
Case G	CA	0.0125	0.1
Case H	CA	0.05	0.14

Table 2. Parameters of strut geometry (variation of AR while maintaining constant perimeter).

Geometry case	Cross-sectional shape	AR	Strut height h (mm)	Strut width w (mm)
Case A	RT	2	0.05	0.1
Case I	RT	4	0.03	0.12
Case J	CA	2	0.06	0.12
Case K	CA	4	0.035	0.14

The present work addresses this gap by conducting a parametric computational fluid dynamics (CFD) study of strut cross-sectional shapes, widths, heights, and ARs under consistent boundary conditions. This approach enables direct and mechanistically consistent comparison of haemodynamic and pharmacokinetic outcomes across designs. The study provides new insight into the trade-off between favourable haemodynamics and effective drug delivery, thereby identifying geometric configurations that can inform the design of next-generation DESs.

2. Materials and Methods

2.1. Mathematical model

In this numerical study, a two-dimensional model of the left anterior descending coronary artery was developed. The computational domain consisted of a single strut and two rectangular regions representing the lumen and tissue domains. The lumen radius was set to R = 1.5 mm [8]. The axial distance along the artery was set to the required length, L = 10 mm, to reach a fully developed flow [15]. The arterial wall thickness was taken as T = 1 mm (see Fig. 1(a)).

The single strut was positioned at the midpoint between the inlet and the outlet. Figure 1(b) shows the two different cross-sectional strut shapes - one non-streamlined and one streamlined - considered in this study. The effects of strut height (h) and width (w) were investigated across eight cases, listed as Cases A to H in Table 1. Cases D and H were included to investigate the impact of increasing strut width compared with Cases A and E. Moreover, to explore the effect of aspect ratio (AR = w/h) while maintaining a constant strut perimeter (equal to Case A), three further models (Cases I to K) were considered, as listed in Table 2. The ranges of strut height, width, and aspect ratio were selected based on previous numerical studies investigating stent geometry [12, 14]. These values are also representative of the characteristic dimensions reported for current DES platforms, which typically feature strut thicknesses in the range of 60-80 μm [16].The artery was assumed symmetric about its centerline, and a symmetry boundary condition was applied at the top of the computational domain, consistent with the simplified modelling assumptions. The configuration represents a long, straight arterial segment with symmetric inlet conditions and a single isolated strut positioned near the wall. Under these conditions, the upper half of the lumen is expected to behave as the mirror image of the lower half, allowing the domain to be reduced to a half-domain without loss of accuracy. The lumen height was chosen to be at least thirty times the strut height, ensuring that recirculation zones remain well-separated from the symmetry plane. This approach minimizes computational cost while preserving the accuracy in near-strut flow and mass transport predictions, consistent with previous studies employing similar assumptions [8, 12, 13].

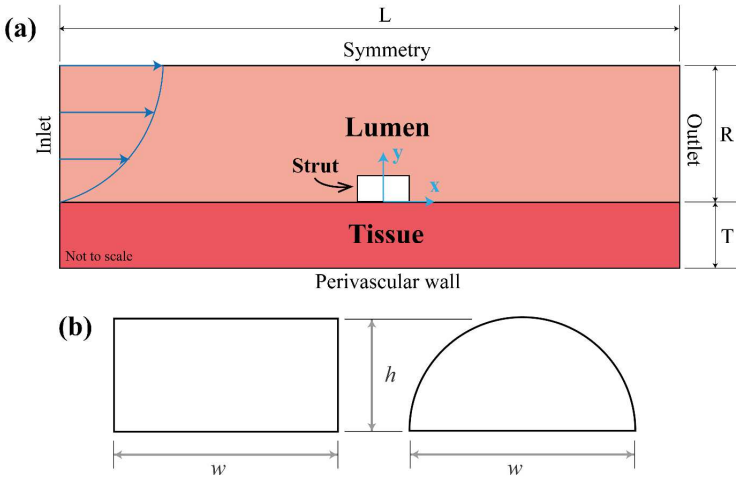

Fig. 1. (a) Schematic diagram of the computational domain depicting a single rectangular strut at the lumen-tissue interface; L, R, and T are respectively the left coronary artery's length, the radius of the arterial lumen, and the tissue thickness, (b) Rectangular (RT) and circular arc (CA) cross-sectional geometric shapes of the strut; w and h represent the strut width and height, respectively.

Luminal blood flow as an incompressible laminar flow follows the continuity and momentum equations:

$$\nabla . \mathbf{v_l} = 0, \tag{1}$$

$$\rho[\mathbf{v_l} . \nabla \mathbf{v_l}] = -\nabla P + \nabla . (\mu \nabla \mathbf{v_l}), \tag{2}$$

where $\mathbf{v_l}$ is the velocity vector of blood in the lumen (m/s), P is the thermodynamic pressure (Pa), $\rho = 1060$ kg/m^3 [9] is the blood density, and $\mu = 0.00345$ Pa.s [9] is the Newtonian blood viscosity. Studies convey that the magnitude of drug uptake in stent-based drug delivery is relatively insensitive to blood rheology [9]. Therefore, assuming blood as a Newtonian fluid would be acceptable. The arterial wall was assumed to behave as a homogenous porous medium. Transport of interstitial fluid in tissue was modeled using the continuity equation and a formulation of the momentum equation, which accounts for the permeability of the arterial wall:

$$\nabla . \mathbf{v_t} = 0, \tag{3}$$

$$\rho[\mathbf{v_t} . \nabla \mathbf{v_t}] = -\nabla P + \nabla . (\mu \nabla \mathbf{v_t}) - \frac{\mu}{K} \mathbf{v_t}. \tag{4}$$

where $\mathbf{v_t}$ is the velocity vector of blood in tissue (m/s), and the permeability coefficient is $K = 1.43 \times 10^{-18}$ m^2 [17]. The steady-state drug transport in the lumen was modeled using an advection-diffusion equation:

$$\mathbf{v_l} . \nabla C = D_l \nabla^2 C, \tag{5}$$

while a diffusion-only equation represented drug transport in the tissue:

$$D_t \nabla^2 C = 0, \tag{6}$$

where C is the normalized drug concentration, defined by the ratio of the local drug concentration, c (kg/m^3), to the concentration of drug on the strut wall, c_0 (kg/m^3):

$$C = \frac{c}{c_0} \tag{7}$$

where D_l and D_t are the diffusion coefficients of the model drug Paclitaxel, with diffusivities in the blood and tissue equal to $D_l = 3.89 \times 10^{-11}$ m^2/s and $D_t = 3.65 \times 10^{-12}$ m^2/s, respectively [8, 18].

2.2. Numerical procedure

A Poiseuille parabolic velocity profile was imposed at the luminal inlet, and a uniform zero-gauge pressure condition was applied at the outlet. The average Reynolds number, Re ~ 282, was calculated by assuming a constant dynamic viscosity $\mu = 0.00345$ Pa.s, and the volumetric mean flow rate in the left anterior descending coronary artery [8, 19]. This low Reynolds number made it possible to model blood flow as laminar. No-slip boundary conditions were applied on the strut-lumen and strut-tissue interfaces. A symmetry boundary condition was specified at the upper boundary of the lumen domain.

For drug transport, a Dirichlet boundary condition was applied by prescribing a normalized drug concentration of unity ($C = 1$) at the strut surfaces, representing a constant drug supply. This simplification defines an upper-bound scenario and enables consistent geometric comparisons. Although real DES coatings release drug in a time-dependent manner, the constant-concentration assumption isolates the geometric effects on drug transport, which is the focus of this study. Continuity of mass flux was ascribed to the lumen-tissue interface. Assuming that the blood enters the domain without any drug, zero concentration ($C = 0$) was imposed at the inlet. The same boundary condition was applied to the perivascular wall, based on the assumption that the drug would not be able to penetrate to the bottom of the tissue. Finally, zero mass flux of the drug was specified on the outlet.

The finite volume solver ANSYS Fluent 2021 R2 (ANSYS Inc.) was used to solve mass and momentum transport equations. Fully structured meshes containing 1.09–1.30 × 10^6 elements (minimum orthogonal quality = 0.98) were sufficient to resolve flow and concentration fields. Figures 2(a) and 2(b) show the mesh-independence study for Cases A and E, respectively. Since mesh independence in this simulation was achieved later for mass transfer equations, each solution was considered mesh-independent when the area-weighted average concentration (AWAC) within a representative tissue region varied by less than 2% between successive refinements. This representative area for all utilized geometries was defined as a rectangle bounded by the upper and lower extents of the tissue domain and the vertical lines $x = -0.5$ mm and $x = 0.5$ mm.

The mesh density was highest near the stent struts and the lumen–tissue interface. This refinement enabled accurate resolution of the thin boundary layers along no-slip boundaries, which include both the stent strut surfaces and the arterial wall. Furthermore, the increased mesh density in these regions facilitated the capture of steep drug concentration gradients around the stent strut and within the tissue. To further substantiate the numerical accuracy, four progressively refined meshes were generated for the representative cases (Cases A and E). Boundary-layer refinement was applied near the strut surfaces and lumen–tissue interface using eight prism (inflation) layers with a growth ratio of 1.2 and a first-cell thickness of 1.0 × 10^{-7} m, ensuring adequate resolution of the viscous sublayer for laminar flow at low Reynolds number. The maximum aspect ratio of elements in the boundary-layer region was kept below 50 to avoid numerical stiffness.

The semi-implicit (SIMPLEC) method coupled the pressure and velocity using a second-order central differencing scheme to discretize the pressure and momentum variables spatially [20]. Other solver settings included a second-order upwind scheme to discretize the drug concentration [21]. Convergence was monitored using scaled residuals, with target reductions of 10^{-6} for continuity and momentum and 10^{-8} for concentration. In addition to residuals, convergence was confirmed when AWAC and representative wall shear stress (WSS) values stabilized to within 0.1% over successive iterations.

Due to the absence of experimental data for direct comparison, the present simulation was validated against a previously published CFD study [9]. The same geometric and boundary conditions were reproduced, and the resulting haemodynamic and drug-delivery parameters closely matched those reported previously, thereby supporting the accuracy and reliability of the current computational approach.

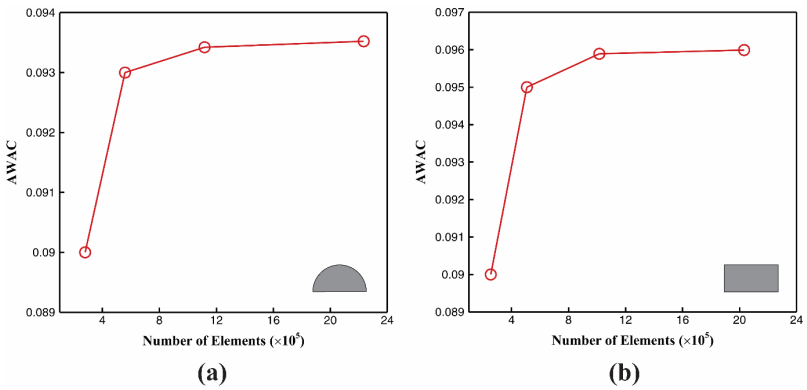

Fig. 2. Mesh-independence study for Cases (a) A and (b) E, showing the AWAC in the tissue region for different grid densities; The third mesh was selected for all simulations, since the variation in AWAC between the last two meshes was less than 2%.

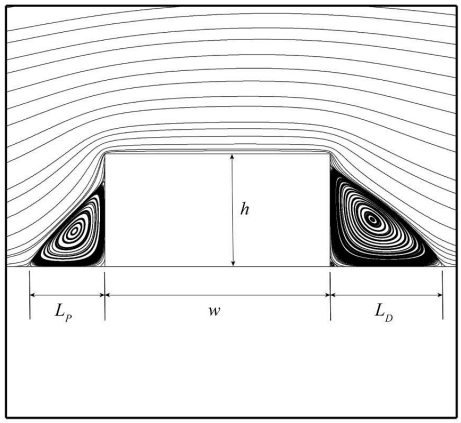

Fig. 3. Proximal and distal recirculation zones surrounding the strut in Case A; L_P and L_D represent the lengths of the proximal and distal recirculation zones, respectively.

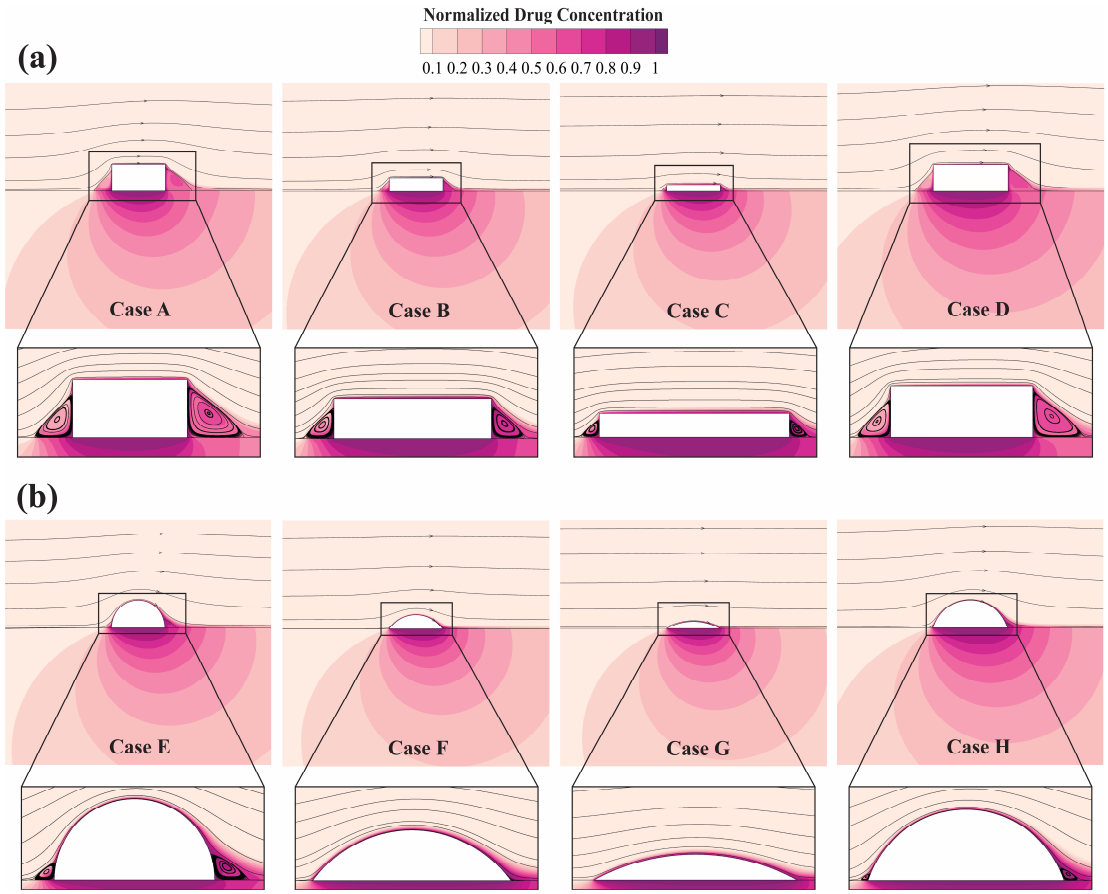

Fig. 4. Normalized drug concentration distribution and flow path lines indicating recirculating flow proximal and distal to the different heights and widths of (a) RT, (b) CA strut shapes.

Table 3. The effects of strut height and width on L_P and L_D.

Geometry Case	L_P (mm)	L_D (mm)
Case A	0.034	0.051
Case B	0.019	0.022
Case C	0.010	0.010
Case D	0.034	0.051
Case E	0.013	0.021
Case F	0	0
Case G	0	0
Case H	0.006	0.011
Case I	0.023	0.027
Case J	0.017	0.028
Case K	0	0

3. Results

3.1. Effects of strut geometry on blood flow

3.1.1. Recirculation length

Each simulation revealed the formation of two distinct recirculation zones, proximal and distal to the strut, upon its entry into the bloodstream. These zones are illustrated in Fig. 3 for Case A. L_P and L_D denote the lengths of the proximal and distal recirculation zones, respectively. Within these regions, consistent with the findings of Kolachalama et al. [8], drug pooling effectively enhances the interaction between the luminal drug and the underlying absorbing vascular tissue. This phenomenon is demonstrated in Fig. 4 for Cases A through H.

Notable recirculation areas are observed in both the proximal and distal regions of Case A, as indicated by the streamlines in Fig. 4. Similar outcomes are observed on both the upstream and downstream sides of Cases B, C, and D. However, for the CA stent strut geometries, flow separation is only observed in Cases E and H. For the flow conditions under investigation, Cases F and G show no evidence of flow separation.

Table 3 displays the recirculation length corresponding to the axial distance of the separation zone (L_P and L_D). The recirculation length decreased as the strut height was reduced, while the strut width remained constant. L_P reduced from 0.034 mm for Case A to 0.010 mm for Case C, which is approximately a 71% decrease. L_D for Case C shrinks by 80% compared to Case A. To compare the RT and CA geometries, Table 3 also shows that L_P and L_D separation lengths decrease by approximately 62% and 59%, respectively, when the geometry is changed from Case A to Case E. In other cases, with RT and CA cross-sections having equal width and height, the reductions in separation zones are even more significant. Notably, the separation length reduces to zero for the CA configurations.

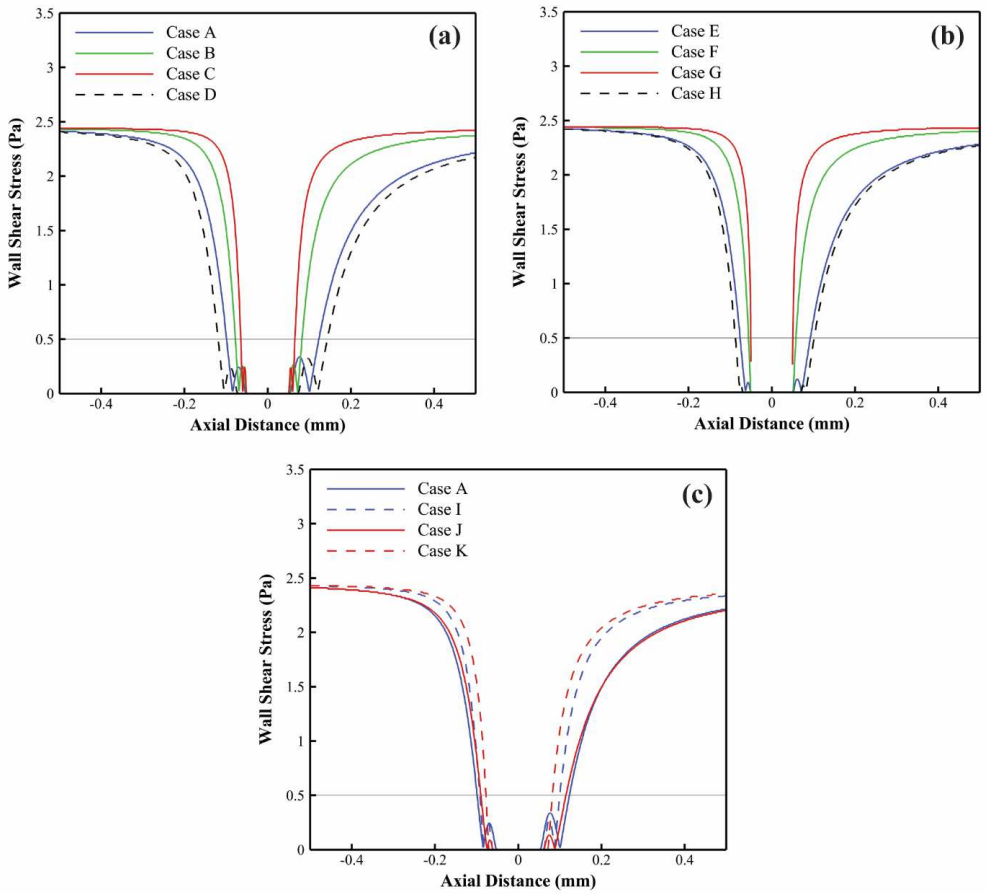

Fig. 5. WSS along the lumen-tissue interface for (a) RT and (b) CA cross-sectional shapes, and (c) for varying ARs.

The effect of width variation was examined by applying a 40% increase in strut width for both geometries in Cases D and H, while maintaining the same height as in Cases A and E. The results indicate that, for the RT cross-section, increasing the width has negligible influence on the recirculation lengths, as evidenced by the similarity between Cases A and D. In contrast, for the CA geometry, L_P and L_D decrease by up to 54% and 48%, respectively, when comparing Cases E and H.

Regarding the effect of AR on separation zones, Table 3 indicates that increasing AR while keeping the strut perimeter constant results in a reduction in recirculation lengths. This reduction is more pronounced in CA strut geometries. Specifically, for CA shapes, the recirculation lengths diminish to zero as AR increases from 2 to 4, as observed in Cases J and K.

3.1.2. *Wall shear stress*

Figure 5 displays the WSS along the lumen-tissue interface for both cross-sectional shapes and the cases listed in Tables 1 and 2. The sections of the artery wall that are susceptible to atherosclerosis and/or intimal thickening are typically identified using a low WSS threshold of 0.5 Pa [18]. Thus, Fig. 5 shows a low WSS threshold of 0.5 Pa. When compared to RT struts, the CA cross-sectional struts resulted in exposure to low WSS that was 44% lower, as illustrated in Figs. 5(a) and 5(b). In both cross-sectional shapes, a decrease in h resulted in a lower percentage of areas with low WSS, consistent with findings from past studies [8, 18]. An increase in w in the RT cross-section resulted in no significant difference in the low WSS area. In the cases of CA shapes, it led to a 28% decline in low WSS percentage.

With respect to changes in AR, Fig. 5(c) illustrates that increasing AR results in a reduction in the percentage of low WSS. For the CA geometry, this reduction was 76% when transitioning from Case J to Case K. In comparison, the RT cross-section showed a 41% decrease in low WSS between Case A and Case I.

3.2. Effects of strut geometry on drug transport

3.2.1. *Spatial drug distribution*

Strut geometry influences local flow disturbances and can also alter convection- and diffusion-driven drug uptake. The effects of height and width variations for both cross-sectional shapes are illustrated in Figs. 6(a) and 6(b). All results are plotted within the tissue, at a depth of one-fifth of the tissue thickness (1/5 T) below the lumen–tissue interface. This approach is consistent with that used by other researchers to analyze spatial drug distribution [18]. Struts with greater height exhibited non-contacting sidewall perimeters together with larger recirculation areas (Table 3), leading to more significant flow-mediated drug uptake. The effect of height changes in circular struts compared to RT ones is stronger. Halving h in a CA (Case E to Case F) resulted in a nearly 10% reduction in drug uptake due to the 26% decrease in the strut perimeter, along with the disappearance of the recirculation zones (Fig. 6(b) and Table 3). In contrast, wider stent struts made more direct contact with the wall, increasing the likelihood of forcing more drug into the wall through only diffusion. A 40% increase in strut width resulted in a 19% enhancement in drug uptake from RT strut (Case D), while this improvement for CA (Case H) was 15% (Figs. 6(a) and 6(b)). The lesser enhancement for CA struts was due to the 23.5% smaller perimeter, plus the diminishing of recirculation zones as a consequence of increasing strut width.

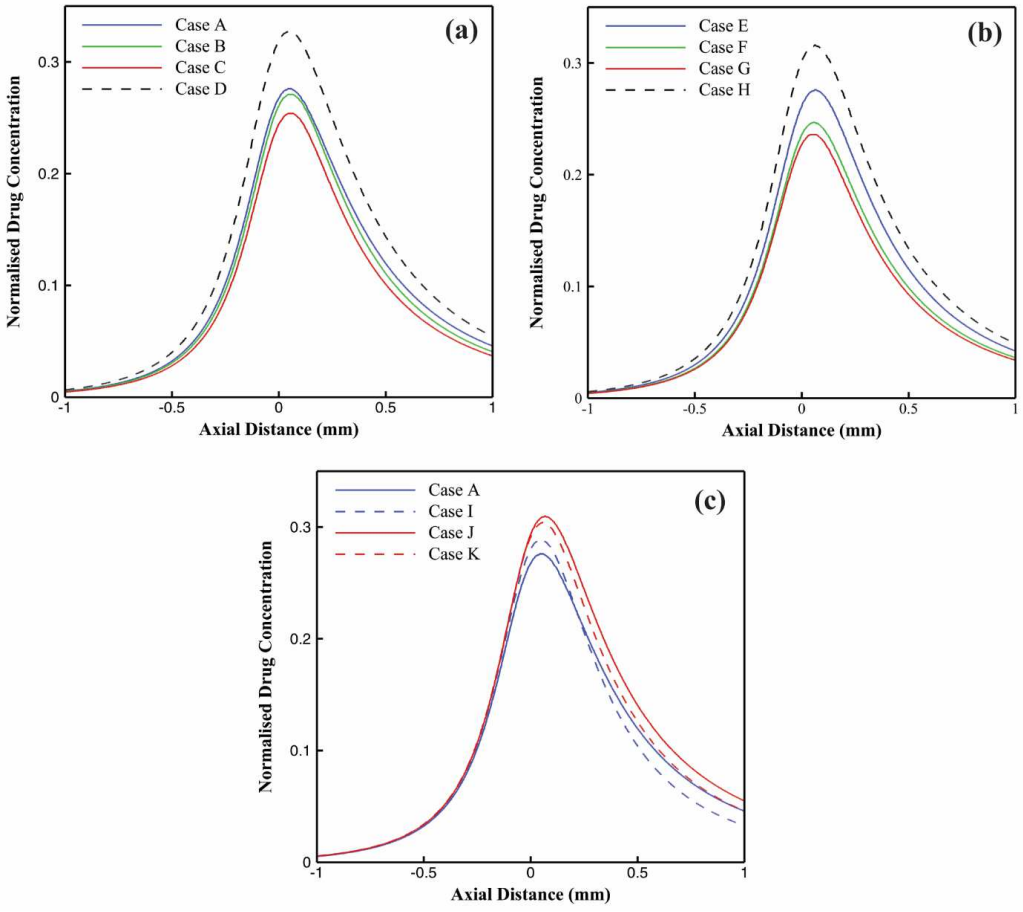

Fig. 6. Effects of strut cross-section on the spatial drug distribution in the tissue measured at a distance $\frac{1}{5}$T below the lumen-tissue interface for (a) RT and (b) CA cross-sectional shapes, and (c) varying ARs.

The AR simulation results, where each strut geometry maintained a constant perimeter, offered further insights into the relative contributions of apposed and non-apposed strut surfaces to overall drug uptake. Drug distribution patterns for streamlined and non-streamlined strut shapes with AR values of 2 (Cases A and I) and 4 (Cases J and K) are illustrated in Fig. 6(c). The findings indicate that, when the strut perimeter is held constant, CA cross-sections result in greater drug uptake compared to RT ones. Although RT struts demonstrated improved performance with increasing AR, the opposite trend was observed for CA struts. Specifically, as the AR of CA struts increased from Case J to Case K, the disappearance of recirculation zones led to a reduction in flow-mediated drug transport, thereby decreasing overall drug uptake (Table 3 and Fig. 6). For cases with equal strut perimeter (Table 2), the distribution of perimeter between the lumen-facing and tissue-facing surfaces is not constant. The CA struts with AR of 2 (Case J) and 4 (Case K) maintain relatively larger tissue-facing contact lengths, whereas the RT struts (Cases A and I) exhibit notable non-contacting regions. This geometric difference influences the mechanisms of drug uptake: a larger tissue-facing contact length enhances direct diffusion-mediated delivery, while a smaller contact length increases dependence on flow-mediated transport. Consequently, Case I, compared with Case A, demonstrates higher drug uptake due to its increased tissue-facing length. Additionally, although Case I has a shorter L_P, an approximately 50% reduction in L_D substantially decreases drug washout, thereby enhancing flow-mediated drug uptake. For CA geometries (Cases J and K), although Case K possesses a longer tissue-facing contact length, the disappearance of recirculation zones results in lower overall drug uptake.

3.2.2. Area-weighted average concentration of drug

Similar to drug distribution in the arterial tissue, the AWAC of the drug depends on strut geometry as well, as evident in Fig. 7. For both strut shapes, higher stent struts resulted in higher AWAC. The decrease in AWAC for the CA strut, as the height changed from h to h/2 (from Case E to Case F), was noticeable, almost 12%. As mentioned before, this decrease occurred due to the noticeable reduction in strut perimeter along with the disappearance of the recirculation zones (Table 3 and Fig. 7(a)). A similar trend was observed for an increase in width. However, this impact was less remarkable in RT cross-sections.

When comparing the effects of AR under constant perimeter conditions, the CA strut with AR = 2 (Case J) produced the highest AWAC. For RT struts, increasing the AR from 2 to 4 (Cases A → I) yielded only a marginal improvement in AWAC. This modest increase can be attributed to the greater tissue-facing contact length in Case I, which enhanced diffusion-mediated uptake, combined with a notable reduction in L_D that minimized drug washout. Although Case I exhibited a slightly shorter L_P, its overall flow-mediated transport was more efficient than in Case A. For CA struts, however, increasing AR from 2 to 4 (Cases J → K) led to diminished drug delivery, as the disappearance of recirculation zones outweighed the limited benefit of the longer tissue-facing surface.

4. Discussion and Limitations

The present study provides a comprehensive parametric analysis of how strut geometric features, namely height, width, cross-sectional shape, and aspect ratio, influence near-wall haemodynamics and drug transport in an idealized coronary stent configuration. The results demonstrate that even minor geometric modifications can substantially alter recirculation dynamics, WSS, and drug uptake within the arterial wall.

4.1. Influence of strut geometry on haemodynamics and drug transport

Strut height plays a pivotal role in determining both the extent of flow separation and the resulting drug delivery performance. Increasing the strut height enlarged upstream and downstream recirculation zones, producing extended regions of low WSS (< 0.5 Pa). These separated flow regions enhance flow-mediated drug delivery by increasing residence time but simultaneously expose the endothelium to low-shear environments linked to thrombosis and restenosis. Conversely, shorter struts reduce recirculation and restore more physiological shear patterns, though with slightly reduced drug uptake. Thus, height governs a fundamental trade-off between haemodynamic stability and delivery efficiency.

Strut width also influenced drug transport behaviour by altering the diffusion-dominated component of delivery. Wider struts expanded the contact area between the polymer coating and the tissue, enhancing diffusion-mediated transport, but in non-streamlined shapes, this increase also broadened low-WSS regions. Streamlined geometries were less sensitive to width changes, as the smoother flow reattachment limited separation. These results suggest that moderate width achieves a balance between effective diffusion and acceptable flow disturbance.

The cross-sectional shape strongly modulated both haemodynamics and pharmacokinetics. CA profiles facilitated smoother flow over the strut, reducing flow separation and low-WSS exposure. However, the reduced recirculation in these shapes limited flow-mediated transport compared with RT struts, which exhibited greater drug retention but more disturbed flow. Consequently, cross-sectional geometry defines a key design trade-off: streamlined shapes promote vascular healing, while non-streamlined shapes favour drug delivery.

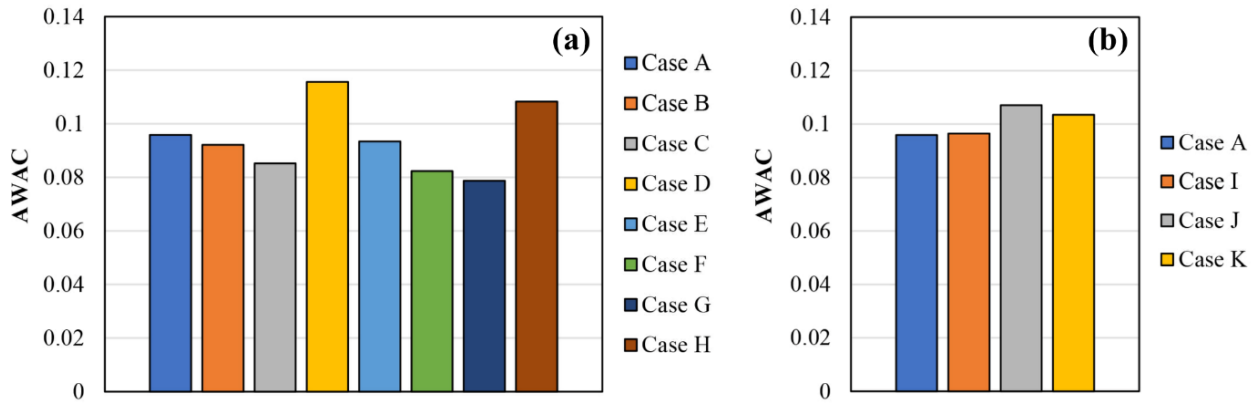

Fig. 7. The effects of strut (a) height and width, and (b) AR on the AWAC within the tissue.

When comparing AR effects at constant perimeter, variations in AR changed both the curvature of the leading edge and the distribution of perimeter length between the lumen- and tissue-facing surfaces. This redistribution directly affected the balance between contact-mediated and flow-mediated transport. Struts with larger tissue-facing contact areas favoured diffusion-mediated delivery, whereas those with smaller contact areas relied more on recirculation-driven mechanisms. Among RT struts (Cases A and I), Case I achieved higher drug uptake due to its longer tissue contact and reduced L_D, which limited washout. For CA struts, a moderate AR = 2 (Case J) provided the highest AWAC by balancing diffusion- and flow-driven effects. Increasing AR further (Case K) flattened the curvature, suppressed recirculation, and reduced drug uptake. These results confirm that equal perimeter does not equate to equal functional contact length; the geometric distribution of that perimeter critically determines transport efficiency.

The CA strut with AR = 2 identified in this study shows flow and transport characteristics consistent with the evolution of modern DES designs, which increasingly employ rounded or arc-shaped struts (e.g., Resolute Onyx, Orsiro, and Xience platforms) [22–24] . Although the absolute dimensions in this simplified two-dimensional model differ from real stent struts, the observed trend toward smoother, thinner, and more streamlined geometries aligns with clinical and manufacturing efforts to enhance deliverability, fatigue resistance, and endothelialization.

4.2. Model simplifications and scope of applicability

This study employed a two-dimensional, single-strut model under steady laminar flow. These simplifications were chosen to enable systematic evaluation of geometric effects while maintaining computational robustness. However, clinical reality involves three-dimensional vessel geometries, multi-strut scaffolds, and pulsatile blood flow, all of which can modify local haemodynamics and drug transport.

In three-dimensional configurations, circumferential flow around strut edges reduces recirculation persistence, meaning the recirculation lengths (L_P, L_D) reported here represent upper-bound estimates. Side-edge bypassing can also increase washout of drug-rich zones, decreasing AWAC compared with two-dimensional predictions. In multi-strut scaffolds, neighboring struts may either amplify or suppress flow disturbances depending on spacing and alignment. Overlapping recirculation zones may enhance residence time, while streamlined multi-strut layouts tend to diminish separation and reduce flow-mediated delivery.

Pulsatile coronary flow introduces further complexity: flow deceleration phases enlarge recirculation zones and transiently increase drug pooling, whereas acceleration phases promote washout. The net effect on AWAC thus depends on waveform, Womersley number, and flow amplitude. The assumption of constant drug concentration at the strut surface represents an upper-bound condition; in practice, drug release decays over time. Although this simplification may overestimate absolute tissue concentrations, it isolates geometric influences, enabling meaningful comparison between cases.

Accordingly, the present results are best interpreted as relative mechanistic insights rather than absolute quantitative predictions. While quantitative values of L_P, L_D, and AWAC would differ under pulsatile or three-dimensional conditions, the qualitative trends are expected to remain valid: taller and non-streamlined struts enhance flow-mediated uptake, whereas streamlined, thinner designs improve haemodynamics at the cost of reduced drug retention. These trends are consistent with prior three-dimensional and pulsatile-flow studies [8–10,12,13,18]. Future work should extend the current framework to include pulsatile flow, multi-strut interactions, and realistic vessel geometries to refine quantitative predictions and guide the design of next-generation DES.

5. Conclusion

This study systematically examined how strut geometry affects near-wall flow and drug transport in an idealized stented artery. The findings show that stent-induced flow disturbances, though often considered adverse, can act as tunable design features for enhancing drug delivery when appropriately managed. Streamlined and non-streamlined designs exhibit opposing characteristics: streamlined profiles reduce disturbed flow and low-WSS regions, improving haemodynamic safety but limiting flow-mediated drug uptake, while non-streamlined profiles enhance uptake at the expense of disturbed flow. Among the configurations with equal perimeter, the CA strut with AR = 2 (Case J) achieved the highest AWAC but exhibited slightly larger low-WSS regions than Case K, demonstrating the intrinsic trade-off between maximizing drug uptake and maintaining physiological shear conditions. Accordingly, Case J may be optimal for drug delivery, whereas Case K offers a more balanced compromise between drug uptake and haemodynamic safety. Although AWAC and WSS were analyzed independently, a composite performance index that integrates drug transport efficiency and haemodynamic metrics would provide a more comprehensive framework for stent optimization. Developing such an index, supported by experimental or clinical data, represents an important avenue for future research. Overall, these results emphasize that stent geometry must be tailored to balance competing objectives of efficient drug delivery, favourable haemodynamics, and mechanical durability. The insights presented here align with ongoing clinical trends toward smoother, thinner, and arc-shaped struts, which not only enhance flow behaviour but also facilitate manufacturing and promote endothelialization. While the present findings stem from a simplified two-dimensional steady model, the qualitative mechanisms identified are expected to persist under more realistic pulsatile and three-dimensional conditions, guiding the rational design of next-generation DESs that optimize both haemodynamic safety and therapeutic efficacy.

Author Contributions

K. Kasaeinia and A. Seyedhosseini planned the scheme, initiated the project, suggested the numerical method, developed the mathematical modelling, and examined the theory validation; R. Mohammadi supervised the project. R. Mohammadi, P.R.S. Vijayaratnam and T.J. Barber discussed the results. The manuscript was written through the contribution of all authors. All authors discussed the results, reviewed, and approved the final version of the manuscript.

Acknowledgments

Not applicable.

Conflict of Interest

The authors declared no potential conflicts of interest concerning the research, authorship, and publication of this article.

Funding

The authors received no financial support for the research, authorship, and publication of this article.

Data Availability Statements

The datasets generated and/or analyzed during the current study are available from the corresponding author on reasonable request.

Nomenclature

AWAC	Area-weighted average concentration	L_P	Length of proximal recirculation zone [mm]
L	Arterial length	c	Local drug concentration [kg/m^3]
T	Arterial wall thickness [mm]	c_0	Local drug concentration on the strut wall [kg/m^3]
AR	Aspect ratio	R	Lumen radius [mm]
ρ	Blood density [kg/m^3]	C	Normalized drug concentration
v_l	Blood velocity in the lumen [m/s]	K	Permeability coefficient [m^2]
v_t	Blood velocity in the tissue [m/s]	Re	Reynolds number
μ	Blood viscosity [Pa.s]	h	Strut height [mm]
D_l	Diffusion coefficient in the blood [m^2/s]	w	Strut length [mm]
D_t	Diffusion coefficient in the tissue [m^2/s]	P	Thermodynamic pressure [Pa]
L_D	Length of distal recirculation zone [mm]	WSS	Wall Shear Stress [Pa]

References

[1] Mukheja, Y., Sarkar, A., Arora, R., Pal, K., Ahuja, A., Vashishth, A., Kuhad, A., Chopra,K., Jain, M., Unravelling the progress and potential of drug-eluting stents and drug-coated balloons in cardiological insurgencies, *Life Sciences*, 352, 2024, 122908.

[2] Song, L., Guan, C., Yu, M., Sun, Z., Fu, G., He, Y., Jia, S., Chen, J., Qi, F., Bai, J., li, W., Ge, J., Han, Y., Gao, R., Sirolimus-eluting iron bioresorbable scaffold versus cobalt-chromium everolimus-eluting stents in patients with coronary artery disease: Rationale and design of the IRONMAN-II trial, *American Heart Journal*, 275, 2024, 53–61.

[3] Vahedi, S.M., Azaiez, J., Optimization of polymer coating thickness and strut width in drug Eluting stents using Magnetic field, *European Journal of Pharmaceutics and Biopharmaceutics*, 203, 2024, 114455.

[4] Vijayaratnam, P.R.S., Reizes, J.A., Barber, T.J., The impact of strut profile geometry and malapposition on the haemodynamics and drug-transport behaviour of arteries treated with drug-eluting stents, *International Journal of Numerical Methods for Heat & Fluid Flow*, 32, 2022, 3881–3907.

[5] Balakrishnan, B., Tzafriri, A.R., Seifert, P., Groothuis, A., Rogers, C., Edelman, B.R., Strut position, blood flow, and drug deposition: implications for single and overlapping drug-eluting stents, *Circulation*, 111, 2005, 2958–2965.

[6] Ma, X., Oyamada, S., Gao, F., Wu, T., Robich, M.P., Wu, H., Wang, X., Buchholz, B., McCarthy, S., Gu, Z., Bianchi, C.F., Sellke, F.W., Laham, R., Paclitaxel/sirolimus combination coated drug-eluting stent: In vitro and in vivo drug release studies, *Journal of Pharmaceutical and Biomedical Analysis*, 54, 2011, 807–811.

[7] Zhang, Y., Yu, H., Deng, L., Hou, Z., Yang, J., Fang, F., Miao, M.Z., Li, W., Shen, X., Hao, D., Ma, X., Zhou, L., He, F., Liu, X., Tacrolimus combined with arsenic trioxide provides a three-in-one drug-eluting coronary stent integrating anti-restenosis, pro-endothelialization and anti-inflammation, *Medicine Novel Technology Devices*, 21, 2024, 100289.

[8] Kolachalama, V.B., Tzafriri, A.R., Arifin, D.Y., Edelman, E.R., Luminal flow patterns dictate arterial drug deposition in stent-based delivery, *Journal of Controlled Release*, 133, 2009, 24–30.

[9] Vijayaratnam, P.R.S., O'Brien, C.C., Reizes, J.A., Barber, T.J., Edelman, E.R., The impact of blood rheology on drug transport in stented arteries: Steady simulations, *PLoS One*, 10, 2015, e012817.

[10] Kasaeinia, K., Mohammadi, R., Seyedhosseini, A., Effect of Blood Rheology on Haemodynamics and Stent-based Drug Delivery for Coronary Arteries, *European Journal of Mechanics - B/Fluids*, 113, 2025, 204282.

[11] Morton, A.C., Crossman, Gunn, D.J., The influence of physical stent parameters upon restenosis, *Pathologie Biologie*, 52, 2004, 196–205.

[12] Jiménez, J.M., Davies, P.F., Hemodynamically driven stent strut design, *Annals of Biomedical Engineering*, 37, 2009, 1483–1494.

[13] Mejia, J., Ruzzeh, B., Mongrain, R., Leask, R., Bertrand, O.F., Evaluation of the effect of stent strut profile on shear stress distribution using statistical moments, *Biomedical Engineering Online*, 8, 2009, 1–10.

[14] Jiang, Y., Zhang, J., Zhao, W., Influence of strut cross-section of stents on local hemodynamics in stented arteries, *Chinese Journal of Mechanical Engineering (English Edition)*, 29, 2016, 624–632.

[15] Deen, W.M., *Analysis of transport phenomena*, Oxford University Press, 1998.

[16] Leone, A., Simonetti, F., Avvedimento, M., Angellotti, D., Immobile Molaro, M., Franzone, A., Esposito, G., Piccolo, R., Ultrathin Struts Drug-Eluting Stents: A State-of-the-Art Review, *Journal of Personalized Medicine*, 12, 2022, 1378.

[17] Tada, S., Tarbell, J.M., Flow through internal elastic lamina affects shear stress on smooth muscle cells (3D simulations), *American Journal of Physiology-Heart and Circulatory Physiology*, 282, 2002, H576-84.

[18] O'Brien, C.C., Kolachalama, V.B., Barber, T.J., Simmons, A., Edelman, E.R., Impact of flow pulsatility on arterial drug distribution in stent-based therapy, *Journal of Controlled Release*, 168, 2013, 115–124.

[19] Kim, H.J., Vignon-Clementel, I.E., Coogan, J.S., Figueroa, C.A., Jansen, K.E., Taylor, C.A., Patient-specific modeling of blood flow and pressure in human coronary arteries, *Annals of Biomedical Engineering*, 38, 2010, 3195–3209.

[20] Van Doormaal, J.P., Raithby, G.D., Enhancements of the simple method for predicting incompressible fluid flows, *Numerical Heat Transfer*, 7, 1984, 147-163

[21] Kolachalama, V.B., Bressloff, N.W., Nair, P.B., Mining data from hemodynamic simulations via Bayesian emulation, *Biomedical Engineering Online*, 6, 2007, 47.

[22] Orsiro Mission | Orsiro US, (n.d.). https://us.orsiro.com/orsiromission (accessed October 27, 2025).

[23] XIENCE Skypoint Ordering Information | Abbott, (n.d.). https://www.cardiovascular.abbott/us/en/hcp/products/percutaneous-coronary-intervention/xience-family/xience-skypoint/ordering-information.html (accessed October 27, 2025).

[24] Resolute Onyx TM DES, (n.d.).

ORCID iD

Kimiya Kasaeinia https://orcid.org/0009-0000-9591-6350
Rafat Mohammadi https://orcid.org/0000-0003-3675-4851
Ali Seyedhosseini https://orcid.org/0009-0003-6042-8834
Pujith R.S. Vijayaratnam https://orcid.org/0000-0002-1219-0169
Tracie J. Barber https://orcid.org/0000-0002-6574-8074

How to cite this article: Kasaeinia K., et al., Influence of Strut Cross-section on Haemodynamics and Drug Transport in Stent-based Therapy, *J. Appl. Comput. Mech.*, xx(x), 2026, 1–10. https://doi.org/10.22055/jacm.2026.48692.5432